The Astrophysical Journal, 709:436–446, 2010 January 20 doi:10.1088/0004-637X/709/1/436

SPIN-DOWN MEASUREMENT OF PSR J1852+0040 IN KESTEVEN 79: CENTRAL COMPACT OBJECTS AS ANTI-MAGNETARS

J. P. Halpern and E. V. Gotthelf
Columbia Astrophysics Laboratory, Columbia University, New York, NY 10027, USA
Received 2009 October 25; accepted 2009 December 7; published 2009 December 31

ABSTRACT

Using *XMM-Newton* and *Chandra*, we achieved phase-connected timing of the 105 ms X-ray pulsar PSR J1852+0040 that provides the first measurement of the spin-down rate of a member of the class of central compact objects (CCOs) in supernova remnants. We measure $\dot{P} = (8.68 \pm 0.09) \times 10^{-18}$, and find no evidence for timing noise or variations in X-ray flux over 4.8 year. In the dipole spin-down formalism, this implies a surface magnetic field strength $B_s = 3.1 \times 10^{10}$ G, the smallest ever measured for a young neutron star, and consistent with being a fossil field. In combination with upper limits on B_s from other CCO pulsars, this is strong evidence in favor of the "anti-magnetar" explanation for their low luminosity and lack of magnetospheric activity or synchrotron nebulae. While this dipole field is small, it can prevent accretion of sufficient fall-back material so that the observed X-ray luminosity of $L_x = 5.3 \times 10^{33} (d/7.1\ \mathrm{kpc})^2$ erg s^{-1} must instead be residual cooling. The spin-down luminosity of PSR J1852+0040, $\dot{E} = 3.0 \times 10^{32}$ erg s^{-1}, is an order of magnitude smaller than L_x. Fitting of the X-ray spectrum to two blackbodies finds small emitting radii, $R_1 = 1.9$ km and $R_2 = 0.45$ km, for components of $kT_1 = 0.30$ keV and $kT_2 = 0.52$ keV, respectively. Such small, hot regions are ubiquitous among CCOs, and are not yet understood in the context of the anti-magnetar picture because anisotropic surface temperature is usually attributed to the effects of strong magnetic fields.

Key words: ISM: individual objects (Kes 79) – pulsars: individual (PSR J0821-4300, 1E 1207.4-5209, PSR J1852+0040) – stars: neutron

Online-only material: color figures

1. INTRODUCTION

The class of relatively faint X-ray sources known as central compact objects (CCOs) in supernova remnants (SNRs) is apparently isolated neutron stars, which we define here by their steady flux, predominantly thermal X-ray emission, lack of optical or radio counterparts, and the absence of a surrounding pulsar wind nebula (see reviews by Pavlov et al. 2004 and De Luca 2008). Table 1 lists basic data on the well-studied CCOs, as well as candidates whose qualifications are not well established. Of the seven most secure members, three are definitely pulsars with periods of 0.105, 0.112, and 0.424 s (Gotthelf et al. 2005; Gotthelf & Halpern 2009; Zavlin et al. 2000). Until now, no spin-down was detected from a CCO, which is most simply interpreted as indicating a weak surface dipole magnetic field B_s. In two cases, PSR J1852+0040 ($P = 0.105$ s) and 1E 1207.4−5209 ($P = 0.424$ s), the *upper limits* on B_s from spin period measurements are 1.5×10^{11} G and 3.3×10^{11} G, respectively (Halpern et al. 2007; Gotthelf & Halpern 2007), smaller than that of any other young neutron star. We also found $B_s < 9.8 \times 10^{11}$ G from a pair of observations of PSR J0821−4300, the 0.112 s pulsar in Puppis A (Gotthelf & Halpern 2009).

Important implications of these results are that the birth periods of the CCO pulsars are not significantly different from their present values, and that their spin-down luminosities are, and have always been, insufficient to generate significant non-thermal magnetospheric emission or synchrotron nebulae. A corollary is that the so-called "characteristic age" $\tau_c \equiv P/2\dot{P}$ that is used to approximate the true age of pulsar has, for CCOs, no meaning, being at least millions of years for pulsars that are demonstrably in SNRs that are only a few thousand years old. It is also reasonable to suppose that some isolated radio pulsars with weak magnetic fields that have characteristic ages of millions of years may actually be former CCOs that are only moderately aged.

Most of the properties of the CCOs can thus be explained by an "anti-magnetar" model (Halpern et al. 2007; Gotthelf & Halpern 2008), including the possibility that their weak magnetic fields are causally related to their slow rotation periods at birth through the turbulent dynamo (Thompson & Duncan 1993) that generates the magnetic field. (See Spruit 2008 for a review of possible mechanisms for the origin of magnetic fields in neutron stars.) While CCOs are inconspicuous relative to ordinary young pulsars and magnetars, the fact that they are found in SNRs in comparable numbers to other classes of neutron stars implies that they must represent a significant fraction of neutron star births. Considering that the CCO in Cassiopeia A is the youngest known neutron star (330 year), and postulating that a CCO in SN 1987A explains why its pulsar has not yet been detected, argues that anti-magnetars are potentially a populous class.

The compact X-ray source CXOU J185238.6+004020 was discovered in the center of the SNR Kes 79 by Seward et al. (2003). In previous papers, we reported the discovery of 105 ms pulsations from that CCO, now named PSR J1852+0040 (Gotthelf et al. 2005, Paper I), and the first few observations that established only an upper limit on its period derivative corresponding to $B_s < 1.5 \times 10^{11}$ G (Halpern et al. 2007, Paper II). Here, we present a dedicated series of timing observations of PSR J1852+0040 that constitute the first definite measurement of the spin-down rate of a CCO pulsar, confirming its unusually small dipole magnetic field and supporting the anti-magnetar model. The plan that was devised to obtain the needed series of time-constrained observations is described in Section 2. Analysis and results of the timing data are presented in Section 2.1,

Table 1
Central Compact Objects in Supernova Remnants

CCO	SNR	Age (kyr)	d (kpc)	P (s)	f_p[a] (%)	B_s (10^{11} G)	$L_{x,\mathrm{bol}}$ (erg s^{-1})	References
RX J0822.0 − 4300	Puppis A	3.7	2.2	0.112	11	<9.8	6.5×10^{33}	1, 2
CXOU J085201.4 − 461753	G266.1 − 1.2	1	1	···	<7	···	2.5×10^{32}	3, 4, 5, 6, 7
1E 1207.4 − 5209	PKS 1209 − 51/52	7	2.2	0.424	9	<3.3	2.5×10^{33}	8, 9, 10, 11, 12
CXOU J160103.1 − 513353	G330.2 + 1.0	$\gtrsim$3	5	···	<40	···	1.5×10^{33}	13, 14
1WGA J1713.4 − 3949	G347.3 − 0.5	1.6	1.3	···	<7	···	$\sim 1 \times 10^{33}$	7, 15, 16
CXOU J185238.6 + 004020	Kes 79	7	7	0.105	64	0.31	5.3×10^{33}	17, 18, 19, 20
CXOU J232327.9 + 584842	Cas A	0.33	3.4	···	<12	···	4.7×10^{33}	20, 21, 22, 23, 24
XMMU J172054.5 − 372652	G350.1 − 0.3	0.9	4.5	···	···	···	3.4×10^{33}	25
XMMU J173203.3 − 344518	G353.6 − 0.7	∼27	3.2	···	···	···	1.0×10^{34}	26, 27, 28
CXOU J181852.0 − 150213	G15.9 + 0.2	1 − 3	(8.5)	···	···	···	$\sim 1 \times 10^{33}$	29

Notes. Above the line are seven well-established CCOs. Below the line are three candidates.
[a] Upper limits on pulsed fraction are for a search down to $P = 12$ ms or smaller.
References. (1) Hui & Becker 2006; (2) Gotthelf & Halpern 2009; (3) Slane et al. 2001; (4) Kargaltsev et al. 2002; (5) Bamba et al. 2005; (6) Iyudin et al. 2005; (7) De Luca 2008; (8) Zavlin et al. 2000; (9) Mereghetti et al. 2002a; (10) Bignami et al. 2003; (11) De Luca et al. 2004; (12) Gotthelf & Halpern 2007; (13) Park et al. 2006; (14) Park et al. 2009; (15) Lazendic et al. 2003; (16) Cassam-Chenaï et al. 2004; (17) Seward et al. 2003; (18) Gotthelf et al. 2005; (19) Halpern et al. 2007; (20) this paper; (21) Pavlov et al. 2000; (22) Chakrabarty et al. 2001; (23) Mereghetti et al. 2002b; (24) Pavlov & Luna 2009; (25) Gaensler et al. 2008; (26) Tian et al. 2008; (27) Acero et al. 2009; (28) Halpern & Gotthelf 2009; (29) Reynolds et al. 2006.

and the high-quality X-ray spectrum and pulse profile that were obtained from the summed observations are the subject of Section 2.2. Discussion of the anti-magnetar model and possible explanations for the X-ray spectrum appear in Section 3, followed by the conclusions in Section 4.

In this paper, we adopt a distance of 7.1 kpc to Kes 79 from H I and OH absorption studies (Frail & Clifton 1989; Green & Dewdney 1992) updated using the Galactic rotation curve of Case & Bhattacharya (1998). We also assume the dynamical estimate of 5.4–7.5 kyr for the age of the SNR from Sun et al. (2004).

2. X-RAY OBSERVATIONS

After the first four timing observations of PSR J1852+0040 in 2004 and 2006 (Paper II), it was evident that the frequency derivative $\dot{f}$ was too small to measure without obtaining a phase-coherent series of observations spanning several years. The most economical way to measure $\dot{f}$ is to begin with a logarithmically spaced sequence of observations that maintains the absolute cycle count $\phi(t)/2\pi$ and measures the frequency f with increasing accuracy, until the small quadratic term in the phase ephemeris

$$\frac{\phi(t)}{2\pi} = f(t - t_0) + \frac{1}{2}\dot{f}(t - t_0)^2 + \cdots$$

begins to make a significant contribution to the phase. In this case, it was also deemed possible (Paper II) that accretion from fall-back material could contribute timing irregularities known as torque noise, of a magnitude comparable to the existing upper limits on dipole spin-down. This made it all the more important to obtain a well-sampled ephemeris that could test for such effects.

Unfortunately, maintaining cycle count would require more observations classified as time-constrained than the *Chandra X-ray Observatory* allocates to any one project, while for *XMM-Newton*, semiannual visibility windows for this source are only 40 days long, not wide enough to securely bridge over the intervening five month gaps. It took until 2008 to implement a strategy that uses the two satellites in a coordinated fashion, filling two *XMM-Newton* visibility windows with six observations each of variable spacing, while requesting pairs of *Chandra* observations to bridge the gaps between and after the two *XMM-Newton* windows. In this manner, a phase-coherent timing solution spanning 1.7 year could be achieved, which could also be extrapolated backward to incorporate the earlier observations. All but one of the approved observations in 2008–2009 were performed as planned. Due to a loss of contact with the *XMM-Newton* spacecraft, the last observation of 2008 was rescheduled to 2009, but this did not compromise the success of the program. We were thus able to obtain a fully coherent timing solution incorporating all of the observations listed in Table 2, including the earliest ones, spanning 4.8 year in total.

All of the *XMM-Newton* observations used the pn detector of the European Photon Imaging Camera (EPIC-pn) in "small window" (SW) mode to achieve 5.7 ms time resolution, and an absolute uncertainty of ≈3 ms on the arrival time of any photon. We processed all EPIC data using the emchain and epchain scripts under Science Analysis System (SAS) version xmmsas_20060628_1801-7.0.0. The leap second at the end of 2008 was inserted manually. Simultaneous data were acquired with the EPIC MOS cameras, operated in "full frame" mode. Although not useful for timing purposes because of the 2.7 s readout, the location of the source at the center of the on-axis MOS CCDs allows a better background measurement to test for flux variability, an important indicator of accretion, than the EPIC-pn SW mode.

The *Chandra* observations used the Advanced Camera for Imaging and Spectroscopy (ACIS) in continuous-clocking (CC) mode to provide time resolution of 2.85 ms. This study uses data processed by the pipeline software revisions v7.6.9–v8.0. Reduction and analysis used the standard software package CIAO (v3.4) and CALDB (v3.4.2). The photon arrival times in CC mode are adjusted in the standard processing to account for the known position of the pulsar, spacecraft dither, and SIM offset. Absolute accuracy of the time assignment in *Chandra* CC-mode is limited by the uncertainty in the position of the pulsar, which was determined in Paper II from an ACIS image. The typical accuracy of ≈1 pixel then corresponds to an uncertainty of ≈3 ms, which is similar to the *XMM-Newton*

Table 2
Log of X-ray Timing Observations of PSR J1852+0040

Mission	Instr/Mode	ObsID/Sequence No.	Date (UT)	Exposure (ks)	Start Epoch (MJD)	Period[a] (ms)	Z_3^2
XMM-Newton	EPIC-pn/SW	0204970201	2004 Oct 18	30.6	53296.001	104.912638(39)	121.7
XMM-Newton	EPIC-pn/SW	0204970301	2004 Oct 23	30.5	53301.984	104.912612(55)	77.2
XMM-Newton	EPIC-pn/SW	0400390201	2006 Oct 08	29.7	54016.245	104.912610(47)	92.4
Chandra	ACIS-S3/CC	6676/500630	2006 Nov 23	32.2	54062.256	104.912592(40)	94.0
XMM-Newton	EPIC-pn/SW	0400390301	2007 Mar 20	30.5	54179.878	104.912600(43)	107.5
Chandra	ACIS-S3/CC	9101/500964	2007 Nov 12	33.1	54426.674	104.912615(40)	95.8
Chandra	ACIS-S3/CC	9102/500965	2008 Jun 16	31.2	54628.080	104.912593(40)	115.5
XMM-Newton	EPIC-pn/SW	0550670201	2008 Sep 19	21.2	54728.758	104.912563(84)	61.7
XMM-Newton	EPIC-pn/SW	0550670301	2008 Sep 21	31.0	54730.066	104.912594(46)	84.2
XMM-Newton	EPIC-pn/SW	0550670401	2008 Sep 23	34.8	54732.079	104.912573(42)	80.3
XMM-Newton	EPIC-pn/SW	0550670501	2008 Sep 29	33.0	54738.016	104.912596(40)	97.4
XMM-Newton	EPIC-pn/SW	0550670601	2008 Oct 10	36.0	54750.006	104.912641(40)	90.0
Chandra	ACIS-S3/CC	9823/501015	2008 Nov 21	30.1	54791.803	104.912645(55)	69.8
Chandra	ACIS-S3/CC	9824/501016	2009 Feb 20	29.6	54882.483	104.912591(53)	80.4
XMM-Newton	EPIC-pn/SW	0550671001	2009 Mar 16	27.0	54906.255	104.912610(48)	97.9
XMM-Newton	EPIC-pn/SW	0550670901	2009 Mar 17	26.0	54907.609	104.912592(60)	82.9
XMM-Newton	EPIC-pn/SW	0550671201	2009 Mar 23	27.3	54913.582	104.912616(46)	104.8
XMM-Newton	EPIC-pn/SW	0550671101	2009 Mar 25	19.9	54915.654	104.912544(85)	75.8
XMM-Newton	EPIC-pn/SW	0550671301	2009 Apr 04	26.0	54925.539	104.912590(52)	97.9
XMM-Newton	EPIC-pn/SW	0550671901	2009 Apr 10	30.5	54931.535	104.912620(48)	82.9
XMM-Newton	EPIC-pn/SW	0550671801	2009 Apr 22	28.0	54943.897	104.912621(69)	67.4
Chandra	ACIS-S3/CC	10128/501055	2009 Jun 02	33.2	54984.888	104.912596(37)	117.9
Chandra	ACIS-S3/CC	10129/501056	2009 Jul 29	32.2	55041.231	104.912633(40)	105.6

Note [a] Barycentric period derived from a Z_3^2 test. The Leahy et al. (1983) uncertainty on the last digits is in parentheses.

accuracy, and is 0.03 rotations in the case of PSR J1852+0040. We will show that the measured dispersion in pulse arrival times is comparable to this uncertainty.

2.1. Results of Timing Analysis

For each observation in Table 2, we transformed the photon arrival times to Barycentric dynamical time (TDB) using the pulsar coordinates determined in Paper II and reproduced in Table 3. Diffuse SNR emission is a significant source of background. To maximize the pulsar signal-to-noise ratio, we used a source extraction radius of 12″ for the *XMM-Newton* observations, and five columns (2.″4) for the *Chandra* CC-mode data. An energy cut of 1–5 keV was found to maximize pulsed power. The pulse profile and value of the period in each observation was derived from a Z_3^2 periodogram (Buccheri et al. 1983), a choice of harmonics that was found to minimize the uncertainties. The resulting profiles were cross-correlated, shifted, and summed to create a master pulse profile template. Individual profiles were then cross-correlated with the template to determine the time of arrival (TOA) at each epoch.

Starting with the dense series of *XMM-Newton* observations in 2008 September, the TOAs were iteratively fitted using the TEMPO[1] software. We fitted the three observations from September 19–23 to a linear ephemeris and added TOAs one at a time using a quadratic ephemeris, finding that the new TOA would match to <0.1 cycles the predicted phase derived from the previous set. After adding the final observation to the ephemeris, we then worked backward in time from 2008 September to 2004 October until all 23 observations had been included. The quadratic term contributes −8.7 cycles of rotation over the 4.8 year span of the ephemeris, which yields the small uncertainty in $\dot{P}$ discussed below. The phases and errors were determined by cross-correlating with a final iterated template of co-added profiles produced from the best-fitting ephemeris given in Table 3. Figure 1 shows the residuals of the individual observations from the best fit, which demonstrates the validity of the solution. The weighted rms of the phase residuals is 3.4 ms, or 0.032 pulse cycles, which is comparable to the individual measurement errors. There is no evidence of timing noise or higher derivatives in the residuals. The variation of Z_3^2 (pulsed power) among the observations listed in Table 2 is also consistent with statistical expectations. Figure 2 shows the summed pulse profile from the 16 *XMM-Newton* observations, for which it is possible to measure a reasonably accurate background (unlike the *Chandra* CC-mode data).

The sensitivity of the results to $\dot{P}$ and B_s can be estimated analytically. If a pulsar is spinning down smoothly, then a coherent timing solution spanning time T will have an uncertainty

Table 3
Spin Parameters of PSR J1852+0040

Parameter	Value
R.A. (J2000)[a]	$18^h52^m38^s.57$
Decl. (J2000)[a]	+00°40′19.″8
Epoch (MJD TDB)[b]	54597.00000046
Spin period, P	0.104912611147(4) s
Period derivative, $\dot{P}$	$(8.68 \pm 0.09) \times 10^{-18}$
Valid range of dates (MJD)	53296–55041
Surface dipole magnetic field, B_s	3.1×10^{10} G
Spin-down luminosity, $\dot{E}$	3.0×10^{32} erg s^{-1}
Characteristic age, τ_c	192 Myr

Notes.
[a] Measured from *Chandra* ACIS-I ObsID 1982 (Paper I). Typical *Chandra* ACIS coordinate uncertainty is 0.″6.
[b] Epoch of ephemeris corresponds to phase zero in Figure 2.

[1] http://www.atnf.csiro.au/research/pulsar/tempo

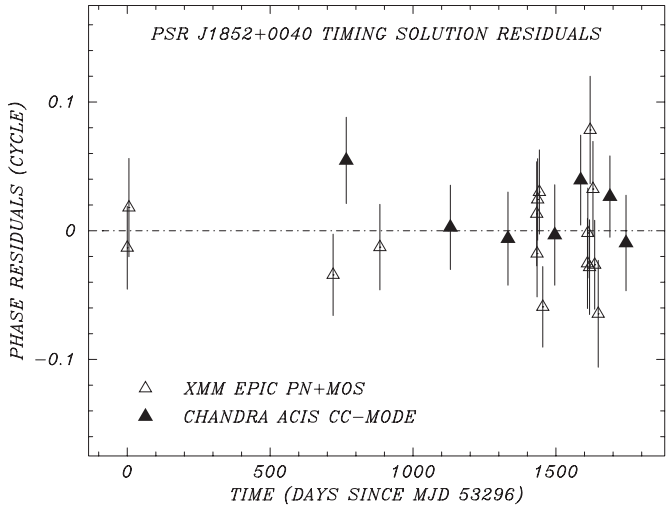

Figure 1. Pulse phase residuals for the 23 timing observations of PSR J1852+0040 from the best-fitting ephemeris of Table 3. Error bars are 1σ.

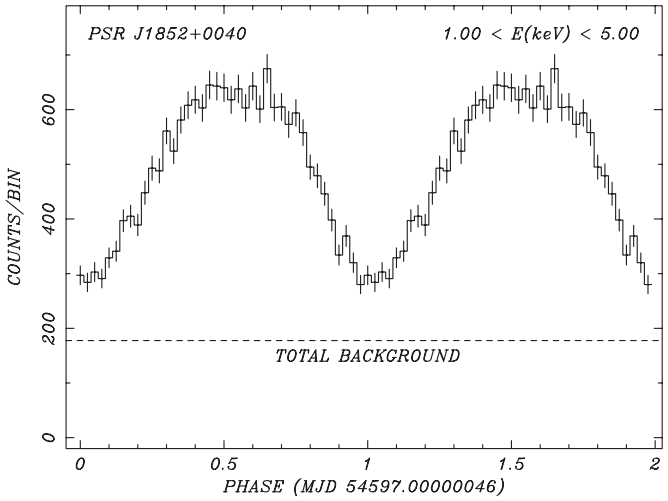

Figure 2. Summed pulse profile from the 16 *XMM-Newton* observations of PSR J1852+0040 listed in Table 2, folded using the ephemeris of Table 3. Phase zero corresponds to the TDB epoch in Table 3. The pulsed fraction after correcting for background is $f_p = 64\% \pm 2\%$.

in frequency of $\delta f = \delta P/P^2 \approx 0.1/T$ and will be sensitive to a period derivative of $\dot{P}_{\rm min} = \delta\dot{P} \approx 0.2(P/T)^2$. This in turn will measure $B_s = 3.2 \times 10^{19}\sqrt{P\dot{P}}$ with fractional uncertainty

$$\frac{\delta B_s}{B_s} \approx 1.0 \times 10^{38}\,\frac{P^3}{B_s^2\,T^2} = 0.05\left(\frac{B_s}{10^{10}\,\mathrm{G}}\right)^{-2}\left(\frac{T}{4.8\ \mathrm{yr}}\right)^{-2} \times \left(\frac{P}{0.105\ \mathrm{s}}\right)^{3}.$$

A coherent ephemeris for PSR J1852+0040 spanning 4.8 year has an uncertainty on $\dot{P}$ of $\delta\dot{P} \approx 1 \times 10^{-19}$, corresponding to a 5σ detection limit of $B_s = 5 \times 10^9$ G. In comparison, the measured values $P = 0.104912611147(4)$ s and $\dot{P} = 8.68(9) \times 10^{-18}$ have fitted uncertainties consistent with these analytic estimates, and imply in the dipole spindown formalism a surface magnetic field strength $B_s = 3.1 \times 10^{10}$ G, a spin-down luminosity $\dot{E} = -I\Omega\dot{\Omega} = 4\pi^2 I\dot{P}/P^3 = 3.0 \times 10^{32}$ erg s^{-1}, and characteristic age $\tau_c \equiv P/2\dot{P} = 192$ Myr, all with negligible statistical error.

2.2. Flux and Spectral Analysis

In Papers I and II, we presented several observations of PSR J1852+0040 that were consistent with steady flux and a blackbody spectrum of $kT \approx 0.46$ keV. The luminosity of $3.4 \times 10^{33}\,d_{7.1}^2$ erg s^{-1} corresponded to a blackbody radius of only $\approx 0.8\,d_{7.1}$ km. This is typical result for a CCO, and indicates a concentrated hot spot that remains to be understood. Using the methods described in Paper I, we now combine all 16 *XMM-Newton* observations of PSR J1852+0040 into one spectrum in order to search for deviations from a blackbody that might indicate temperature variations on the surface, or cyclotron lines. EPIC pn and MOS spectra were fitted jointly. The accumulated exposure allows us to fit the spectrum over 0.7–7 keV, an increase in coverage over the 1–5 keV range used in the previous papers. While a single blackbody can still be fitted with a temperature of 0.46 keV, the high signal-to-noise ratio and expanded energy range of the summed spectrum reveal systematic deviations from the fit; the reduced $\chi^2_\nu = 1.38$ for 240 degrees of freedom is unacceptable (see Figure 3 and Table 4). Similar to the results from other CCOs, we find that a fit to two blackbodies is significantly improved ($\chi^2_\nu = 1.07$), with temperatures of $kT_1 = 0.30$ keV and $kT_2 = 0.52$ keV, while the corresponding radii $R_1 = 1.9\,d_{7.1}$ km and $R_2 = 0.45\,d_{7.1}$ km still cover only a small fraction of the surface. Here we define radius using the phase-averaged luminosity $L_{1,2} = 4\pi R_{1,2}^2 \sigma T_{1,2}^4$ regardless of the unknown emission geometry, which could be, for example, a concentric annulus. Adoption of the two-blackbody fit results in a higher bolometric luminosity than the single blackbody, $5.3 \times 10^{33}\,d_{7.1}^2$ erg s^{-1} versus $3.0 \times 10^{33}\,d_{7.1}^2$ erg s^{-1}. We do not combine the *Chandra* spectra here for an independent fit because of the increased background and other uncertainties involved in analyzing CC-mode data for this faint source.

Additional spectral models that were explored include the nonmagnetic neutron star hydrogen atmosphere of Zavlin et al. (1996), and a simplified Comptonized blackbody, as described by Halpern et al. (2008) for application to anomalous X-ray pulsars. Each of these models fits nearly as well as the two-blackbody model because they can eliminate the residual excess at high energy that is left by a single blackbody fit (see Figure 4 and Table 4). For the neutron star atmosphere (NSA), we fixed the parameters $M = 1.4\,M_\odot$ and $R^\infty = 13.06$ km (corresponding to $R = 10$ km), treating the effective temperature and distance as free parameters. As expected, the fitted temperature is smaller than those of the blackbody models, but the fitted distance of 23.7 kpc is a factor of 3.3 higher than the known value. This indicates that in the atmosphere model only $\sim$10% of the surface is emitting. We are not motivated to search for an atmosphere model that fits to the full surface area, as was done for the Cas A CCO by Ho & Heinke (2009), because the larged pulsed fraction of PSR J1852+0040 clearly requires a small hot spot. The same interpretation attaches to the Comptonized blackbody model, in which the inferred blackbody radius is only $0.93\,d_{7.1}$ km.

The large intrinsic pulsed fraction, $f_p = 64\% \pm 2\%$ (defined as the fraction of counts above the minimum in the light-curve, corrected for background; see Figure 2) confirms that the emitting area must be small and far from the rotation axis, while the line of sight also makes a large angle to the rotation axis. The pulse shape does not appear to be a function of energy (Figure 5), which also suggests that the emitting area is small. The fitted column density from any model in Table 4 agrees reasonably

Table 4
XMM-Newton Spectral Fits to PSR J1852+0040

Parameter	BB	BB+BB	NSA	Comp BB
$N_{\rm H}$ (10^{22} cm^{-2})	1.32 ± 0.05	$1.82^{+0.23}_{-0.18}$	$1.67^{+0.06}_{-0.07}$	$1.53^{+0.09}_{-0.08}$
kT_1 (keV)	0.460 ± 0.007	0.30 ± 0.05	0.287 ± 0.007	0.396 ± 0.014
R_1 (km)	$0.72\, d_{7.1}$	$1.9\, d_{7.1}$	13.06[a]	$0.93\, d_{7.1}$
kT_2 (keV)	...	0.52 ± 0.03	...	...
R_2 (km)	...	$0.45\, d_{7.1}$	...	...
Γ	...	...	...	$4.80^{+0.34}_{-0.25}$
d (kpc)	...	...	$23.7^{+4.0}_{-2.6}$	...
$F_x(0.5-10$ keV)[b]	2.0×10^{-13}	2.0×10^{-13}	2.0×10^{-13}	2.0×10^{-13}
$L_{\rm bol}$ (erg s^{-1})[c]	$3.0 \times 10^{33}\, d_{7.1}^2$	$5.3 \times 10^{33}\, d_{7.1}^2$	...	$3.6 \times 10^{33}\, d_{7.1}^2$
$\chi^2_\nu(\nu)$	1.38(204)	1.07(201)	1.10(204)	1.12(203)

Notes. Spectrum fitted over 0.7–7 keV. Errors are 90% confidence for one interesting parameter ($\chi^2 = \chi^2_{\rm min} + 2.7$).
[a] Fixed parameter $R^\infty = 13.06$ km corresponding to $R = 10$ km with $M = 1.4\, M_\odot$.
[b] Absorbed flux in units of erg cm^{-2} s^{-1}. Average of EPIC pn and MOS.
[c] Unabsorbed, bolometric luminosity assuming $d = 7.1$ kpc. Average of EPIC pn and MOS.

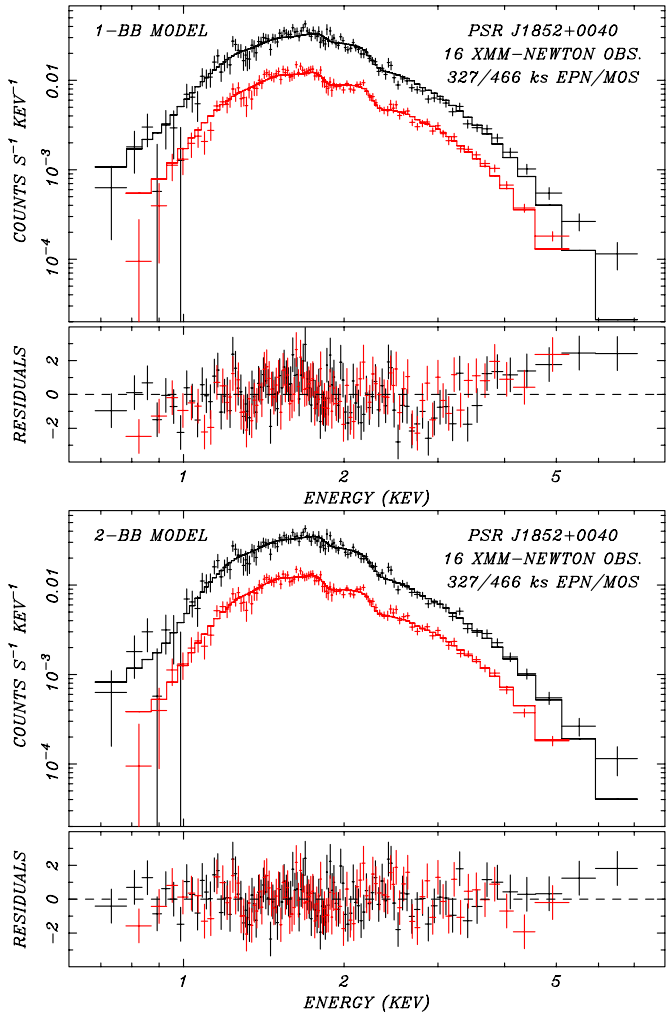

Figure 3. Spectrum of the 16 summed *XMM-Newton* observations of PSR J1852+0040. The EPIC pn spectrum is black, while the average of the MOS1 and MOS2 spectra is red. Top: fit to a single blackbody model. Bottom: fit to a double blackbody model. The parameters of the fits are given in Table 4.

(A color version of this figure is available in the online journal.)

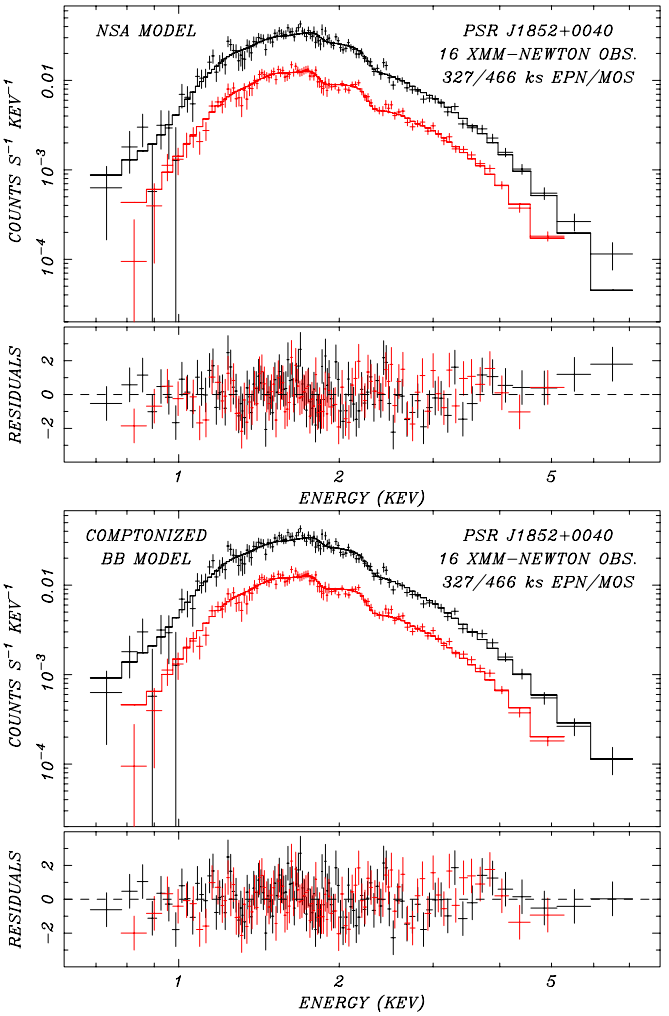

Figure 4. Spectrum of the 16 summed *XMM-Newton* observations of PSR J1852+0040. The EPIC pn spectrum is black, while the average of the MOS1 and MOS2 spectra is red. Top: fit to a nonmagnetic neutron star hydrogen atmosphere model. Bottom: fit to a Comptonized blackbody model. The parameters of the fits are given in Table 4.

(A color version of this figure is available in the online journal.)

well with the $N_{\rm H}$ derived from fits to the SNR spectrum. Sun et al. (2004) find $N_{\rm H} = (1.54$–$1.78) \times 10^{22}$ cm^{-2} from fitting a variety of equilibrium and non-equilibrium ionization models to *ASCA* and *Chandra* spectra of the SNR, while Giacani et al. (2009) find $N_{\rm H} = (1.52 \pm 0.02) \times 10^{22}$ cm^{-2} from fitting a non-equilibrium ionization model to the *XMM-Newton* observations of 2004.

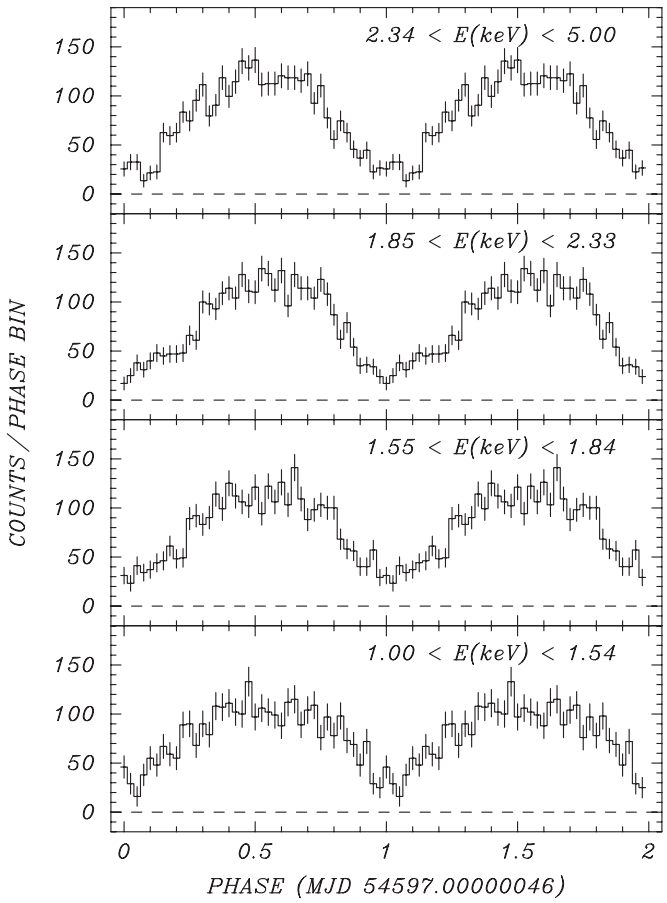

Figure 5. Energy-resolved pulse profiles from the summed 16 *XMM-Newton* observations of PSR J1852+0040 of Figure 2 decomposed into four energy bands containing equal numbers of photons. Background has been subtracted. The pulse shape does not differ significantly as a function of energy.

We then searched for any indication of variability by extracting and fitting the spectrum of each individual observation, fixing the spectral parameters (except for the total flux) to those of the summed spectrum. In order to minimize statistical and systematic errors in this comparison, we restricted the fitted energy range to 1–5 keV for the individual spectra. The resulting individual fluxes are shown in Figure 6, where they are seen to be constant within errors. The mean 1–5 keV flux is 1.9×10^{-13} erg cm^{-2} s^{-1}. The typical 1σ uncertainty in each observation is ≈10%, and the rms dispersion among the 23 observations is 10%.

Unlike the unique case of 1E 1207.4−5209, there is no evidence for cyclotron absorption lines in the spectrum of PSR J1852+0040 or in any other CCO. 1E 1207.4−5209 has strong absorption features at 0.7 and 1.4 keV (Sanwal et al. 2002; Mereghetti et al. 2002a) that can be attributed to the cyclotron fundamental energy E_c and its first harmonic in a field of $\approx 8 \times 10^{10}$ G (Bignami et al. 2003), according to the relation $E_c = 1.16(B/10^{11}\,\mathrm{G})/(1+z)$ keV, where $z \approx 0.3$ is the gravitational redshift. The spectrum of PSR J1852+0040 can now be understood in terms of its weaker surface B-field. For $B_s = 3.1 \times 10^{10}$ G, the cyclotron fundamental and first harmonic are at 0.27 keV and 0.54 keV, below the region accessible to X-ray spectroscopy (Figure 3), especially because of the larger intervening column density to PSR J1852+0040. The same explanation applied to other well-observed CCOs suggests that they also have weaker surface B-fields than 1E 1207.4−5209.

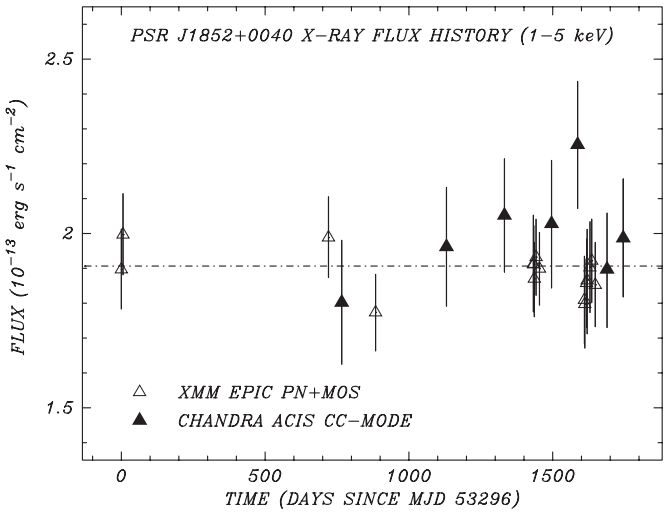

Figure 6. Fluxes in the 1–5 keV band for the 23 individual observations of PSR J1852+0040, fitted to the two blackbody model given in Table 4. Errors bars are 1σ. The weighted mean flux is indicated by the dot-dashed line.

3. DISCUSSION

3.1. CCOs as Anti-magnetars

The steady spin-down of PSR J1852+0040 is consistent with magnetic braking of an isolated neutron star with a weak magnetic field of $B_s = 3.1 \times 10^{10}$ G. In this case, the derived characteristic age of 192 Myr is not meaningful because the pulsar was born spinning at its current period, $P = 0.105$ s, as was the case for the other CCO pulsars, 1E 1207.4−5209 and PSR J0821−4300, which have $P = 0.424$ s and $P = 0.112$ s, respectively. A recent population analysis of radio pulsars by Faucher-Giguère & Kaspi (2006) favors such a wide distribution of birth periods (Gaussian centered on ∼300 ms, $\sigma \sim 150$ ms).

A B-field of this magnitude could be just the fossil field left by flux conservation during the contraction of the core of the progenitor star, as originally hypothesized for neutron stars by Woltjer (1964). Under this hypothesis, CCOs could simply be those neutron stars in which no additional mechanism of B-field amplification has been effective. As stronger fields can be generated by a turbulent dynamo whose strength depends on the rotation rate of the proto-neutron star (Thompson & Duncan 1993), it is natural that pulsars born spinning slowly would have the weaker B-fields. The model of Bonanno et al. (2006) supports this, in particular finding that the B-field of a slowly rotating neutron star should be confined to small-scale regions, while a global dipole that would be responsible for spin-down is absent.

PSR J1852+0040 falls in a region of (P, $\dot{P}$) parameter space (Figure 7) that is devoid of ordinary (non-recycled) radio pulsars (Manchester et al. 2005)[2]. It overlaps with recycled pulsars in this area. The spin parameters of PSR J1852+0040 are not beyond the empirical or theoretical radio pulsar death lines of Faucher-Giguère & Kaspi (2006) or Chen & Ruderman (1993), respectively. One possible explanation for the absence of radio emission from CCOs is low-level accretion of SN debris for thousands or even millions of years. However, the sample of CCOs is not yet large enough to know if they are intrinsically radio quiet.

[2] See also http://www.atnf.csiro.au/research/pulsar/psrcat/.

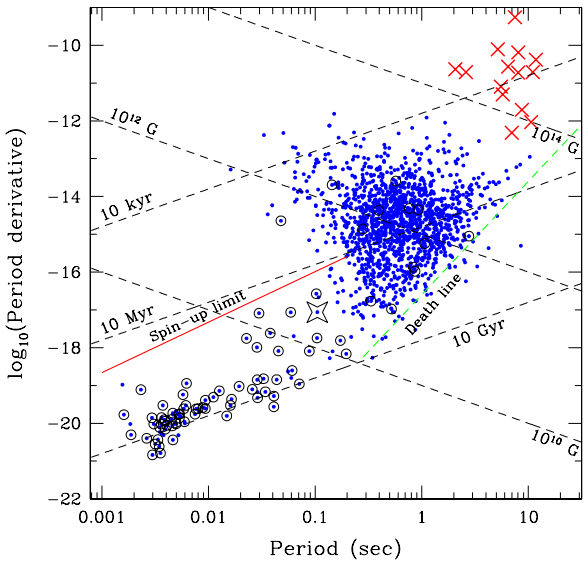

Figure 7. P–$\dot{P}$ diagram of isolated pulsars (dots), binary radio pulsars (circled dots), and magnetars (crosses). The location of PSR J1852+0040 is marked by the star. The radio pulsar death line $B/P^2 = 1.7 \times 10^{11}$ G s^{-2} of Bhattacharya et al. (1992) is indicated. The spin-up limit for recycled pulsars corresponds to $P(\mathrm{ms}) = 1.9\,(B/10^9\,\mathrm{G})^{4/3}$ (van den Heuvel 1987).

(A color version of this figure is available in the online journal.)

Binary pulsars with similar spin parameters as PSR J1852+0040 are thought to have been partly spun up by accretion. It was also suggested by Deshpande et al. (1995) that most single pulsars in this region are recycled, the birth rate of pulsars with $B_s < 10^{11.5}$ G being too low in their estimation, perhaps one in ∼5000 year. Hartman et al. (1997) concluded, to the contrary, that it is not possible to distinguish ordinary pulsars of $B_s = 10^{10.5-11.5}$ from recycled ones, and that there is no reason to suppose that any such single pulsar is recycled. The measurements of spin parameters of CCOs certainly increase the inferred birth rate of neutron stars in this weak B-field regime, a renewed warning not to assume that isolated radio pulsars with similar spin parameters are recycled. It should be expected that many of the ≈52 radio pulsars with $B_s < 10^{11}$ G and 0.1 s $< P <$ 0.7 s in Figure 7 have characteristic ages that are meaningless, being hundreds of millions of years. They have not moved in the (P, $\dot{P}$) diagram and may be former CCOs whose SNRs dissipated only 10^5–10^6 yr ago. Once the SNR has disappeared and the neutron star has cooled, it is difficult to recognize and classify such an "orphan CCO" using X-rays unless it was first selected as a radio pulsar. Allowing for this observational handicap, CCOs having weak B-fields may represent a channel of neutron star birth that is as common as any other.

This outcome is counter in its details to the long debated "injection" hypothesis. Using the "pulsar current" analysis proposed by Phinney & Blandford (1981), Vivekanand & Narayan (1981) and Narayan (1987) suggested that a large fraction of pulsars are injected with 0.5 s $< P <$ 1.0 s and $\dot{P} > 1 \times 10^{-14}$ (i.e., with large magnetic field), or that neutron stars do not turn on as radio pulsars until their $\dot{P}$ decreases below a critical value of $\sim 3 \times 10^{-13}$. This would require that they also cool rapidly in order not to be detected as thermal X-ray sources in SNRs. Later investigators (e.g., Lyne et al. 1985; Lorimer et al. 1993) argued that this interpretation suffers from substantial statistical uncertainties and selection effects in pulsar surveys, and that injection of a distinct population of pulsars is not necessary. While previous authors dismissed the possibility of injection of radio pulsars with weak B-fields (e.g., Srinivasan et al. 1984), this appears to be exactly the origin of radio-quiet CCOs. The related problem of the missing pulsars in empty-shell SNRs (Gotthelf 1998) has largely been solved in recent years through a variety of channels, as summarized by Kaspi & Helfand (2002), including the detection of radio-faint pulsars, pulsar wind nebulae in X-rays, and now, pulsations from CCOs.

The spin-down power $\dot{E} = 3.0 \times 10^{32}$ erg s^{-1} of PSR J1852+0040 is an order of magnitude smaller than its observed thermal X-ray luminosity, $L_x \approx 5.3 \times 10^{33}\, d_{7.1}^2$ erg s^{-1}, which argues that the latter is mostly residual cooling. Remaining questions presented by the X-ray properties of PSR J1852+0040 and other CCOs are focussed on the details of their X-ray spectra and pulse profiles, which require small heated areas. In the case of PSR J1852+0040, the spectrum is more complex than a single blackbody. In the two blackbody model, for example, the hotter component, of temperature $kT_2 = 0.52$ keV, has an area of only $\sim 2.5\, d_{7.1}^2$ km^2. The canonical open-field-line polar cap has area $A_{\mathrm{pc}} = 2\pi^2 R^3/Pc \approx 1.1$ km^2, which is comparable to the area of the hot spot, but polar cap heating by any magnetospheric accelerator must be negligible in this case, being much smaller than the spin-down power. Accretion may cover a wider area and generate more luminosity, but that process is also problematic for PSR J1852+0040, as discussed below. In the remainder of this section, we discuss alternative hypotheses for the weak surface B-fields and thermal hot spots of CCOs, involving internal magnetic fields, anisotropic conduction, and accretion of fall-back material. Although these theories have some attractive properties, they are speculative, and none yet offers a self-consistent explanation for all of the observed properties of CCOs.

3.2. Localized Heating by Magnetic Field Decay?

While the X-ray luminosity of PSR J1852+0040, 5×10^{33} erg s^{-1}, is consistent with minimum neutron star cooling scenarios (Page et al. 2004, 2007) for the age of Kes 79 (5.4–7.5 kyr; Sun et al. 2004), the high temperatures and small surface areas fitted to the X-ray spectrum are difficult to understand without invoking either localized heating on the surface or strongly anisotropic conduction. We recall that the X-ray spectra and luminosities of CCOs are not very different from those of quiescent magnetars, another recently recognized class, being attributable largely to one or two surface thermal emission components (e.g., Halpern & Gotthelf 2005). It is difficult to distinguish CCOs from quiescent magnetars without timing data or evidence about variability (Halpern & Gotthelf 2009). Thus, it is tempting to hypothesize that the same magnetic field decay that is thought to be responsible for localized crustal heating in a magnetar can be operating in CCOs. However, in the case of CCOs, such B-fields would need to have the same 10^{14}–10^{15} G strengths as in magnetars to account for persistent X-ray luminosities of 10^{33}–10^{34} erg s^{-1}, while having insignificant dipole moments that do not contribute to spin-down. One such configuration would be a small "sunspot" dipole on the rotational equator to account for the large pulse modulation, while the rest of the star contributes dipole $B_s < 3 \times 10^{10}$ G in order not to exceed the observed spin-down rate. While we cannot rule out this possibility, it would be remarkable if the magnetic field of a neutron star could be created or evolve into a configuration with such extreme contrast. Also, the conspicuous lack of X-ray variability from CCOs argues against invoking the same magnetic field strength and heating mechanism that is held responsible for magnetars, with their ubiquitous variability.

3.3. Anisotropic Conduction?

We next turn to the possibility that magnetic field confined entirely beneath the surface can be responsible for the nonuniformity of surface temperature. While a strong B-field is a favored ingredient of models for anisotropic conduction, PSR J1852+0040 with its exceptionally weak dipole field would seem the least likely candidate for such an explanation. Nevertheless, it is possible that a strong toroidal field can exist under the surface, while only a weak external poloidal field contributes to spin-down. A toroidal field is expected to be the initial configuration generated by differential rotation in the proto-neutron star dynamo (Thompson & Duncan 1993). The effects on the surface temperature distribution of an internal toroidal field were calculated by Pérez-Azorín et al. (2006), Geppert et al. (2006), and Page et al. (2007). One of the effects of crustal toroidal field is to insulate the magnetic equator from heat conduction, resulting in warm spots at the poles. It was even shown that the warm regions can be of different sizes due to the antisymmetry of the poloidal component of the field, which is reminiscent of the asymmetric opposing thermal regions in the Puppis A CCO (Gotthelf & Halpern 2009).

In order to explain the large observed pulsed fraction of PSR J1852+0040, the axis of toroidal magnetic field must make a large angle with respect to the rotation axis of the neutron star. An orthogonal configuration was in fact adopted by Geppert et al. (2006) and Page et al. (2007). Even if the toroidal field component is initially parallel to the rotation axis, a toroidal field will deform the neutron star into a prolate shape, which tends toward orthogonality to the rotation axis as a minimum energy configuration (Braithwaite 2009). The main problems with this mechanism are (1) anisotropic conduction is unlikely to produce a small hot region on PSR J1852+0040 that covers only $\sim$1% of the surface area of the neutron star, and (2) it does not explain why only one of the orthogonal poles is evidently hot.

Furthermore, to have a significant effect on the heat transport, the crustal toroidal field strength required in these models is $\sim 10^{15}$ G, many orders of magnitude greater than the poloidal field if the latter is measured by the spin-down. Purely toroidal or poloidal fields are thought to be unstable (Tayler 1973; Flowers & Ruderman 1977), although the toroidal field may be stabilized by a poloidal field that is several orders of magnitude smaller (Braithwaite 2009), so this may be a viable configuration for a CCO. On the other hand, twisting and breaking of the crust by such a large toroidal field is the basis of the magnetar model for soft gamma-ray repeaters and anomalous X-ray pulsars (Thompson et al. 2002), which also have large external dipole fields as measured by their rapid spin-down. In this picture, a CCO is a magnetar-in-waiting, a scenario that Pavlov & Luna (2009) found somewhat contrived, as do we. If *any* pulsar *could* be an incipient magnetar, it is not explained why CCOs have especially weak surface fields compared to ordinary pulsars.

3.4. Submergence of Magnetic Field by Hypercritical Accretion?

For as long as the SN explosion mechanism has been studied, it has been noted that a newly born neutron star may accrete large amounts of fall-back material in the hours to months after the SN. This could submerge the initial magnetic field into the core (Geppert et al. 1999), and the surface field could be essentially zero if the accreted matter is not highly magnetized in a well-ordered fashion. After the accretion stops, the submerged field will diffuse back to the surface (Muslimov & Page 1995), but this could take hundreds to millions of years (Geppert et al. 1999). In this picture, the CCOs could be those neutron stars that suffered the most fall-back accretion, while the normal pulsars with ages of a few thousand years must have accreted $\ll 0.01\,M_\odot$. In the model of Muslimov & Page (1995) with accretion of $\sim 10^{-5}\,M_\odot$, the regrowth of the surface field is largely complete after $\sim 10^3$ year, so this would probably not explain the weak field of PSR J1852+0040. But if $>0.01\,M_\odot$ is accreted, then the diffusion time could be millions of years. Chevalier (1989) calculated that the neutron star in SN 1987A could have accreted $\sim 0.1\,M_\odot$ of fallback material in the hours after the SN explosion, aided by a reverse shock from the helium layer of the progenitor. If so, it may never emerge as a radio pulsar. A more normal type II SN should accrete $10^{-3}\,M_\odot$ or less, which may delay the emergence of the magnetic field for tens of thousands of years, a timescale applicable to explaining the properties of CCOs.

Finally, it should be considered that a thermoelectric instability mechanism driven by the strong temperature gradient in the outer crust (Blandford et al. 1983) could regenerate the magnetic field submerged by accretion. However, the growth of the field via this mechanism could take $\sim 10^5$ year. CCOs could then be those neutron stars in which the thermoelectric instability is the dominant mechanism of generating magnetic field, perhaps because their initial rotation rates are slow.

The models discussed here have the effect of delaying the emergence of a normal magnetic field for times ranging from a thousand years to essentially forever. They are difficult to test using CCOs, for which it is impossible to measure the braking index, which could indicate field amplification. Furthermore, they do not help to explain the small, hot surface areas seen in the X-ray spectra of CCOs. In order to achieve such a configuration, the magnetic field would have to be submerged everywhere except for one or two small regions, perhaps the magnetic poles of the neutron star, which could remain hot via conduction from the interior.

3.5. Continuing Accretion from a Fall-back Disk?

We also consider ongoing accretion from a fall-back disk of supernova debris as a possible source of anisotropic surface heating. While variability is an indicator of accretion, we do not have evidence of any variations of PSR J1852+0040 at the 10% level among 23 observations spanning 4.8 year, which would tend to eliminate accretion as a significant contributor to its X-ray luminosity. However, although accretion is widely considered to be an inherently unstable process, it is not clear that variability of X-ray binaries or active galctic nuclei can be extrapolated to accretion from a fossil disk at rates of only $\sim 10^{-5}\,L_{\rm Edd}$. Therefore, we also explore the possibility of accretion, constrained only by the steady spin-down rate of PSR J1852+0040, using the theory of propeller and accretion-disk torques.

The spin parameters of PSR J1852+0040 fall in a regime in which both dipole braking and accretion torques are conceivably significant. In Paper II, we discussed the implications for $\dot{P}$ of PSR J1852+0040 accreting and spinning down in the propeller regime, deriving

$$\dot{P} \approx 2.2 \times 10^{-16}\,\mu_{28}^{8/7}\,\dot{M}_{13}^{3/7}\left(\frac{M}{M_\odot}\right)^{-2/7} I_{45}^{-1}\left(\frac{P}{0.105\ \mathrm{s}}\right) \times \left(1 - \frac{P}{P_{\rm eq}}\right)$$

for the propeller effect. In this model, $\dot{M}$ is the rate of mass expelled, which must be $>\dot{m}$, which is the accretion rate onto the neutron star. We can therefore assume $L_X = \eta \dot{m} c^2$ to calculate a lower limit on $\dot{M}$ in the propeller accretion scenario. Assuming efficiency $\eta \sim 0.1$, $\dot{M} > 5 \times 10^{13}$ g s^{-1} is required. But if we were to adopt $\mu = B_s R^3$, where $B_s = 3.1 \times 10^{10}$ G from assuming dipole spin-down, then the observed $\dot{P} = 8.68 \times 10^{-18}$ allows a negligible $\dot{M} < 3 \times 10^8$ g s^{-1}, which contradicts the accretion assumption.

If instead we use the measured $\dot{P}$ as an upper limit on the propeller spin-down rate, we can derive an upper limit on the required μ in the accretion scenario. Under these assumptions, $\mu < 3.4 \times 10^{26}$ G cm^3, or $B_s < 3.4 \times 10^9$ G. However, this would marginally violate the conditions of the propeller model, because for such a small magnetic field, the magnetospheric radius is

$$r_m = 2.3 \times 10^7 \, \mu_{26}^{4/7} \, \dot{M}_{13}^{-2/7} \left(\frac{M}{M_\odot} \right)^{-1/7} = 2.6 \times 10^7 \text{ cm},$$

which is smaller than the corotation radius

$$r_{\rm co} = (GM)^{1/3} \left(\frac{P}{2\pi} \right)^{2/3} = 3.7 \times 10^7 \text{ cm},$$

and the pulsar would be rotating near its equilibrium period. But there has not been enough time in the life of Kes 79 for a weakly accreting pulsar to come into equilibrium. To find PSR J1852+0040 in an equilibrium state would be a remarkable coincidence because its spin-down timescale, $P/\dot{P} \sim 4 \times 10^8$ yr, is orders of magnitude greater than its age. Therefore, it is more natural to conclude that the small $\dot{P}$ of PSR J1852+0040 is due purely to dipole spin-down, and that it is not accreting. The absence of accretion would also argue against nonuniform surface composition as a cause of the temperature variations. Finally then, none of the possible mechanisms discussed here for hot spots on CCOs is entirely natural and self-consistent.

4. CONCLUSIONS AND FURTHER WORK

Measurement of the spin-down rate of the 105 ms PSR J1852+0040 in Kes 79 was achieved using X-ray observations coordinated between *XMM-Newton* and *Chandra*. The resulting phase-connected ephemeris spanning 4.8 year requires only the first derivatives of the spin frequency, with no measurable timing noise superposed. The straightforward interpretation of this result is dipole spin-down due to a weak surface magnetic field of $B_s = 3.1 \times 10^{10}$ G, the smallest measured for any young neutron star. While this is the first measurement of the spin-down rate of a CCO, upper limits on the period derivatives of 1E 1207.4−5209 and PSR J0821−4300, as well as spectral features in those two, also indicate weak B-fields. The properties of the CCO class were loosely defined in the past, but it is now evident that a weak B-field is the physical reason that a large fraction of the neutron stars were so named. The body of evidence supports the "anti-magnetar" model for the origin of such CCOs: neutron stars born spinning "slowly" may as a result be endowed with only weak magnetic fields. PSR J1852+0040 falls in a region of (B, P) space that overlaps with moderately recycled pulsars. Single radio pulsars with similar spin parameters may therefore be former CCOs rather than recycled, and they may be much younger than their characteristic ages. X-ray observations of pulsars in this region may find evidence of their relative youth via surface thermal emission.

Ongoing timing studies of the CCOs 1E 1207.4−5209 and PSR J0821−4300 will able to measure their spin-down rates and can refine the correspondence between spectral features interpreted as electron cyclotron lines and surface B-field. Those CCOs such as PSR J1852+0040, with no apparent absorption lines, may simply have weaker B-fields than the others by a factor of 2–3, so that the cyclotron resonance is below the soft X-ray band. Considering those CCOs that have not yet been seen to pulse, there is no reason to suppose that they are of a different physical class. Rather, their surface temperature distributions and/or viewing geometries may deliver only weak modulation that happens to fall below the sensitivity of existing data, while deeper observations may succeed in discovering their spins. It would be of great interest to discover pulsations from the CCO in Cas A, the youngest known neutron star, which in all respects is the prototype of the CCO class. At an age of 330 year, it is an order of magnitude younger than the others, while having similar spectral properties (Pavlov & Luna 2009). In our model, its spin parameters were fixed at birth and should conform closely to those of the older CCOs. A recent *Chandra* observation of the Cas A CCO did not detect pulsations (see the Appendix), but the High Resolution Camera (HRC) that was employed lacks energy resolution, a capability that may be crucial in the same way that it was for the *XMM-Newton* discovery of the pulsar in Puppis A (Gotthelf & Halpern 2009).

A remaining theoretical puzzle about CCOs is the origin of their surface temperature anisotropies, in particular, the one or two warm/hot regions that are smaller than the full neutron star surface. The high signal-to-noise spectrum accumulated from PSR J1852+0040 reveals similar temperature structure as the other CCOs. The measured spin-down power of PSR J1852+0040 is too small by an order of magnitude to contribute to these excess emissions. We considered whether accretion of fall-back material can be responsible for this effect, but find it unlikely in the case of PSR J1852+0040 because of its slow, steady spin-down. If other CCOs are found to have similar spin-down properties, the same arguments would apply to them. Therefore, it is important to measure the spin-down rate of PSR J0821−4300, the CCO in Puppis A, and investigate further its apparent phase-dependent emission line at 0.8 keV (Gotthelf & Halpern 2009), which may be indicative of accretion because it is in emission.

The small regions of high surface temperature are properties that CCOs share with magnetars, although most magnetars are hotter and more luminous. The total X-ray luminosities of CCOs are consistent with slow cooling scenarios, and there would be no need to hypothesize a mechanism of magnetic field amplification beyond simple flux freezing if it were not for their strongly anisotropic surface temperature distributions. Paradoxically, the explanations that have been considered for hot spots invoke strong magnetic fields just below the surface, which is exactly the basis of the magnetar model. In this sense, CCOs are potentially magnetars waiting to emerge, or maybe ordinary neutron stars in which the original field was submerged by especially massive fall-back of supernova debris. This is an unsatisfying picture, if only because the contrast between field strength in different regions must be a factor of 10^4 or larger to affect the surface temperature distribution while maintaining the slow spin-down and allowing soft X-ray cyclotron lines. Resolving this essential mystery of the CCOs will undoubtedly generate new insight into the physics of neutron stars.

We thank Fernando Camilo for supplying Figure 7. This investigation is based on observations obtained with *XMM-Newton*, an ESA science mission with instruments and contributions directly funded by ESA Member States and NASA, and *Chandra*. The opportunity to propose a large project that included coordinated observations between *XMM-Newton* and *Chandra* was crucial for the success of this long-term effort. Financial support was provided by NASA through *XMM* grant NNX08AX71G and *Chandra* Awards SAO GO8-9060X, SAO GO9-0058X, and SAO GO9-0080X issued by the *Chandra* X-ray Observatory Center, which is operated by the Smithsonian Astrophysical Observatory for and on behalf of NASA under contract NAS8-03060.

APPENDIX

SEARCH FOR X-RAY PULSATIONS FROM THE CAS A CCO

In this appendix, we report on analysis of a recent *Chandra* observation designed to be the most sensitive yet to search for pulsations from CXOU J232327.9+584842, the CCO in Cas A. But first we summarize the results of previous attempts. Murray et al. (2002) searched a 50 ks *Chandra* HRC observation and identified several candidate periods, but none was confirmed in a follow-up 50 ks observation (Ransom 2002). Pavlov & Luna (2009) found from a *Chandra* ACIS observation taken in the subarray mode $f_p(3\sigma) < 16\%$ for $P > 0.7$ s. That mode is limited by its sampling time of 0.34 s. ACIS in a full-frame mode has a sampling time of 3.2 s, so is only sensitive to periods >6.4 s. For the 1 Ms of data taken in this mode (Huang et al. 2004), we searched the range 6.4 s $\leqslant P \leqslant$ 100 s and $\dot{f} \leqslant 1 \times 10^{-11}$ Hz s^{-1}, corresponding to $\tau_c \geqslant 330$ yr. The resulting upper limit is $f_p < 4\%$ at 99% confidence. Existing *XMM-Newton* data on CXOU J232327.9+584842 are also limited in sensitivity and time resolution, and do not cover the full range of periods spanned by known CCO pulsars. Using an effective exposure of 9.2 ks in the EPIC pn taken in the full-frame mode, Mereghetti et al. (2002b) reported an upper limit of $f_p < 13\%$ for $P > 0.3$ s, and $f_p < 7\%$ for $P > 3$ s. However, these limits may have been underestimated by a factor of 2–3 (see Pavlov & Luna 2009). Our own analysis sets limits of $f_p < 32\%$ for 0.146 ms $< P \leqslant 3$ s and $f_p < 17\%$ for $P > 3$ s from this observation. Improvements in sensitivity and time resolution could be obtained with a longer *XMM-Newton* observation using the EPIC pn in SW mode, as was employed for the other CCO pulsars.

Recently, 487 ks of *Chandra* HRC timing data were obtained over a period of 11 days in 2009 March, of which 433 ks are in the public archive. We searched the public data for pulsations. A total of 11,486 counts were extracted from a circular aperture of radius 1.″2, of which 6% are estimated to be background. We sampled $(f, \dot{f})$ parameter space using the Z_1^2 test, which is an optimal one for a source in which the light curve, presumed to arise from surface thermal emission, is expected to be weakly modulated and quasi-sinusoidal. We limited the search range to $f \leqslant 200$ Hz for $\dot{f} \leqslant 5 \times 10^{-13}$ Hz s^{-1}, $f \leqslant 100$ Hz for $\dot{f} \leqslant 3 \times 10^{-12}$ Hz s^{-1}, and $f \leqslant 10$ Hz for $\dot{f} \leqslant 1 \times 10^{-10}$ Hz s^{-1}, oversampling by a factor of ≈3 in each parameter. This range covers the parameters of all the known CCO pulsars and magnetars. The largest values of Z_1^2 found were ≈40. The theoretical distribution of noise power is exponential with a mean of 2, so the single trial probability that $Z_1^2 > 40$ by chance is 2×10^{-9}. Such a value is expected to arise randomly in the $\sim 2 \times 10^9$ independent trials that were performed, so it is not significant. The expectation value of the intrinsic pulsed fraction is $f_p = (1 + N_b/N_s)\sqrt{2Z_1^2/N}$, where $N_b/N_s = 0.06/0.94$ is the ratio of background to source counts, and $N = N_s + N_b = 11{,}486$ is the total number of counts. In this case, a sinusoidal signal of $f_p = 9.0\%$ would have a 50% probability of giving $Z_1^2 > 40$. However, taking into account the noise, which may either increase or decrease the total power, the 99% upper limit on the Z_1^2 of a true signal in this case is 75 (Groth 1975; Vaughan et al. 1994), corresponding to $f_p < 12.2\%$. On the other hand, these peak power values are somewhat overestimated because we oversampled Fourier space. Finally, then, we adopt an upper limit of $f_p < 12\%$ for $P > 10$ ms in Table 1, which is the lowest limit yet obtained for Cas A over the range of periods that is spanned by the known CCO pulsars.

REFERENCES

Acero, F., Pühlhofer, G., Klochkov, D., Komin, Nu., Gallant, Y., Horns, D., & Santangleo, A. 2009, Proc. 31st ICRC, in press, arXiv:0907.0642
Bamba, A., Yamazaki, R., & Hiraga, J. S. 2005, ApJ, 632, 294
Bhattacharya, D., Wijers, R. A. M. J., Hartman, J. W., & Verbunt, F. 1992, A&A, 254, 198
Bignami, G. F., Caraveo, P. A., De Luca, A., & Mereghetti, S. 2003, Nature, 423, 725
Blandford, R. D., Applegate, J. H., & Hernquist, L. 1983, MNRAS, 204, 1025
Bonanno, A., Urpin, V., & Belvedere, G. 2006, A&A, 451, 1049
Braithwaite, J. 2009, MNRAS, 397, 763
Buccheri, R., et al. 1983, A&A, 128, 245
Case, G. L., & Bhattacharya, D. 1998, ApJ, 504, 761
Cassam-Chenaï, G., Decourchelle, A., Ballet, J., Sauvageot, J.-L., Dubner, G., & Giacani, E. 2004, A&A, 427, 199
Chakrabarty, D., Pivovaroff, M. J., Hernquist, L. E., Heyl, J. S., & Narayan, R. 2001, ApJ, 548, 800
Chen, K., & Ruderman, M. 1993, ApJ, 402, 264
Chevalier, R. A. 1989, ApJ, 346, 847
De Luca, A. 2008, in AIP Conf. Proc. 983, 40 Years of Pulsars: Millisecond Pulsars, Magnetars, and More, ed. C. Bassa et al. (Melville, NY: AIP), 311
De Luca, A., Mereghetti, S., Caraveo, P. A., Moroni, M., Mignani, R. P., & Bignami, G. F. 2004, A&A, 418, 625
Deshpande, A. A., Ramachandran, R., & Srinivasan, G. 1995, JA&A, 16, 53
Faucher-Giguère, C.-A., & Kaspi, V. M. 2006, ApJ, 643, 332
Flowers, E., & Ruderman, M. A. 1977, ApJ, 215, 302
Frail, D. A., & Clifton, T. R. 1989, ApJ, 336, 854
Gaensler, B. M., et al. 2008, ApJ, 680, L37
Geppert, U., Külker, M., & Page, D. 2006, A&A, 457, 937
Geppert, U., Page, D., & Zannias, T. 1999, A&A, 345, 847
Giacani, E., Smith, M. J. S., Dubner, G., Loiseau, N., Castelletti, G., & Paron, S. 2009, A&A, 507, 841
Gotthelf, E. V. 1998, Me. Soc. Astron. Ital., 69, 831
Gotthelf, E. V., & Halpern, J. P. 2007, ApJ, 664, L35
Gotthelf, E. V., & Halpern, J. P. 2008, in AIP Conf. Proc. 983, 40 Years of Pulsars: Millisecond Pulsars, Magnetars, and More, ed. C. Bassa et al. (Melville, NY: AIP), 320
Gotthelf, E. V., & Halpern, J. P. 2009, ApJ, 695, L35
Gotthelf, E. V., Halpern, J. P., & Seward, F. D. 2005, ApJ, 627, 390 (Paper I)
Green, D. A., & Dewdney, P. E. 1992, MNRAS, 254, 686
Groth, E. J. 1975, ApJS, 29, 285
Halpern, J. P., & Gotthelf, E. V. 2005, ApJ, 618, 874
Halpern, J. P., & Gotthelf, E. V. 2009, ApJ, submitted
Halpern, J. P., Gotthelf, E. V., Camilo, F., & Seward, F. D. 2007, ApJ, 665, 1304 (Paper II)
Halpern, J. P., Gotthelf, E. V., Reynolds, S., Ransom, S. M., & Camilo, F. 2008, ApJ, 676, 1178
Hartman, J. W., Portegies Zwart, S., & Verbunt, F. 1997, A&A, 325, 1031
Ho, W. C. G., & Heinke, C. O. 2009, Nature, 462, 71

Huang, U., et al. 2004, ApJ, 615, L115
Hui, C. Y., & Becker, W. 2006, A&A, 454, 543
Iyudin, A. F., Aschenbach, B., Becker, W., Dennerl, K., & Haberl, F. 2005, A&A, 429, 225
Kargaltsev, O., Pavlov, G. G., Sanwal, D., & Garmire, G. P. 2002, ApJ, 580, 1060
Kaspi, V. M., & Helfand, D. J. 2002, in ASP Conf. Ser. 271, Neutron Stars in Supernova Remnants, ed. P. O. Slane & B. M. Gaensler (San Francisco, CA: ASP), 3
Lazendic, J. S., Slane, P. O., Gaensler, B. M., Plucinsky, P. P., Hughes, J. P., Galloway, D. K., & Crawford, F. 2003, ApJ, 593, L27
Leahy, D. A., Elsner, R. F., & Weisskopf, M. C. 1983, ApJ, 272, 256
Lorimer, D. R., Bailes, M., Dewey, R. J., & Harrison, P. A. 1993, MNRAS, 263, 403
Lyne, A., Manchester, R. N., & Taylor, J. H. 1985, MNRAS, 213, 613
Manchester, R. N., Hobbs, G. B., Teoh, A., & Hobbs, M. 2005, AJ, 129, 1993
Mereghetti, S., De Luca, A., Caraveo, P. A., Becker, W., Mignani, R., & Bignami, G. F. 2002a, ApJ, 581, 1280
Mereghetti, S., Tiengo, A., & Israel, G. L. 2002b, ApJ, 569, 275
Murray, S. S., Ransom, S. M., Juda, M., Hwang, U., & Holt, S. S. 2002, ApJ, 566, 1039
Muslimov, A., & Page, D. 1995, ApJ, 400, L77
Narayan, R. 1987, ApJ, 319, 162
Page, D., Geppert, U., & Külker, M. 2007, Ap&SS, 308, 403
Page, D., Lattimer, J., Prakash, M., & Steiner, A. W. 2004, ApJS, 155, 623
Park, S., Kargaltsev, O., Pavlov, G. G., Mori, K., Slane, P. O., Hughes, J. P., Burrows, D. N., & Garmire, G. P. 2009, ApJ, 695, 431
Park, S., Mori, K., Kargaltsev, O., Slane, P. O., Hughes, J. P., Burrows, D. N., Garmire, G. P., & Pavlov, G. G. 2006, ApJ, 653, L37
Pavlov, G. G., & Luna, G. J. M. 2009, ApJ, 703, 910
Pavlov, G. G., Sanwal, D., & Teter, M. A. 2004, in IAU Symp 218, Young Neutron Stars and their Environments, ed. F. Camilo & B. M. Gaensler (San Francisco, CA: ASP), 239
Pavlov, G. G., Zavlin, V. E., Aschenbach, B., Trümper, J., & Sanwal, D. 2000, ApJ, 531, L53
Pérez-Azorín, J. F., Miralles, J. A., & Pons, J. A. 2006, A&A, 451, 1009
Phinney, E. S., & Blandford, R. D. 1981, MNRAS, 194, 137
Ransom, S. M. 2002, in ASP Conf. Ser. 271, Neutron Stars in Supernova Remnants, ed. P. O. Slane & B. M. Gaensler (San Francisco, CA: ASP), 361
Reynolds, S. P., Borkowski, K. J., Hwang, U., Harrus, I., Petre, R., & Dubner, G. 2006, ApJ, 652, L45
Sanwal, D., Pavlov, G. G., Zavlin, V. E., & Teter, M. A. 2002, ApJ, 574, 61
Seward, F. D., Slane, P. O., Smith, R. K., & Sun, M. 2003, ApJ, 584, 414
Slane, P., Hughes, J. P., Edgar, R. J., Plucinsky, P. P., Miyata, E., Tsunemi, H., & Aschenbach, B. 2001, ApJ, 548, 814
Spruit, H. C. 2008, in AIP Conf. Proc. 983, 40 Years of Pulsars: Millisecond Pulsars, Magnetars, and More, ed. C. Bassa et al. (Melville, NY: AIP), 391
Srinivasan, G., Dwarakanath, K. S., & Bhattacharya, D. 1984, JA&A, 5, 403
Sun, M., Seward, F. D., Smith, R. K., & Slane, P. O. 2004, ApJ, 605, 742
Tayler, R. J. 1973, MNRAS, 161, 365
Thompson, C., & Duncan, R. C. 1993, ApJ, 408, 194
Thompson, C., Lyutikov, M., & Kulkarni, S. R. 2002, ApJ, 574, 332
Tian, W. W., Leahy, D. A., Haverkorn, M., & Jiang, B. 2008, ApJ, 679, L85
van den Heuvel, E. P. J. 1987, in IAU Symp. 125, The Origin and Evolution of Neutron Stars, ed. D. J. Helfand & J. Huang (Dordrecht: Reidel), 393
Vaughan, B. A., et al. 1994, ApJ, 435, 362
Vivekanand, M., & Narayan, R. 1981, JA&A, 2, 315
Woltjer, L. 1964, ApJ, 140, 1309
Zavlin, V. E., Pavlov, G. G., Sanwal, D., & Trümper, J. 2000, ApJ, 540, L25
Zavlin, V. E., Pavlov, G. G., & Shibanov, Yu. A. 1996, A&A, 315, 141